Dengue virus harnesses mosquito Syntenin to load and secrete viral RNA into salivary exosomes

Florian Rachenne[1], Laura Di Pietro[1], Félix Rey-Cadilhac[1], Idalba Serrato-Pomar[1], Norman Schneider[1], Lauryne Pruvost[1], Jacques Dainat[1], Audrey Vernet[2], Chantal Cazevieille[3], Aurélie Ancelin[4], Joséphine Lai Kee Him[4], Sander Jansen[5], Jérémy Fraering[6], Laurianne Simon[7], Dorothée Missé[1,8], Marie Morille[7], Philippe Hammann[6], Martial Seveno[9], Kai Dallmeier[5], Éric Marois[10], Julien Pompon[1,11,#]

1 MIVEGEC, Univ. Montpellier, IRD, CNRS, Montpellier, France

2 PHIM, Univ. Montpellier, IRD, Montpellier, France

3 INM, Electronic Microscopy Platform, Saint Eloi Hospital, Montpellier, France

4 CBS, Electronic Microscopy Platform, CNRS, Montpellier, France

5 KU Leuven Department of Microbiology, Immunology and Transplantion, Rega Institute, Laboratory of Molecular Vaccinology & Vaccine Discovery (MVVD), Leuven, Belgium

6 Plateforme Protéomique Strasbourg-Esplanade, CNRS UAR1589, Institut de Biologie Moléculaire et Cellulaire, Université de Strasbourg, France

7 ICGM, Univ. Montpellier, CNRS, ENSCM, Montpellier, France.

8 International Joint Laboratory PRESTO, Chiang Mai University, Thailand

9 Proteomic platform, PPM, Montpellier, France

10 IBMC, Univ. Strasbourg, CNRS, Inserm, Strasbourg, France.

11 Institute of Molecular Biosciences, Mahidol University, Thailand

corresponding author: Julien.pompon@ird.fr

Key words: viral RNA secretion, RNA loading into extracellular vesicles, virus/vector interaction, arboviral transmission, vector salivary glands.

Abstract

Viruses exploit extracellular vesicles (EVs) to transfer infection-enhancing viral RNAs. However, mechanisms underlying viral RNA loading remain elusive. We leveraged our previous discovery that dengue virus secretes transmission-enhancing subgenomic flaviviral RNA (sfRNA) into mosquito salivary EVs to investigate viral RNA loading mechanism. We demonstrate that sfRNA promotes the secretion of sfRNA-containing EVs marked by the mosquito EV biogenesis protein AeSyntenin, by applying microscopy and viral genetic editing in *in vitro* and *in vivo* models. SfRNA interacts intracellularly with mosquito AeSyntenin and this interaction is selectively maintained within EVs as shown by complementary RNA-affinity chromatography and RNA immunoprecipitation, and AI-based prediction. Finally, we used systemic and salivary gland-specific protein depletion to establish a functional role for mosquito AeSyntenin in exosome production and salivary secretion of sfRNA. We propose that sfRNA binds AeSyntenin to drive its selective packaging and release into exosomes, elucidating a mechanism for viral RNA incorporation into EVs.

Introduction

Viruses exploit extracellular vesicles (EVs) to facilitate infection[1,2]. EVs are non-replicative, lipid bilayer structures secreted into the extracellular space and are broadly classified into two main categories: microvesicles (also known as ectosomes), which bud directly from the plasma membrane[3,4], and exosomes, which originate from the endosomal pathway[3,5–7]. Exosome biogenesis involves Syntenin-1-mediated recruitment via two PDZ domains of the Endosomal Sorting Complex Required for Transport (ESCRT) to form intraluminal vesicles (ILVs) within multivesicular bodies (MVBs)[8–10], which subsequently fuse with the plasma membrane to release exosomes[11,12]. EVs are selectively loaded with RNA and act as intercellular carriers, transferring functional RNA molecules between cells[13–16]. Viruses divert EV carriers to package and transfer viral RNAs (complete or fragment viral genome) into other cells, activating various strategies to enhance infection[1]. Although the presence of viral RNA within EVs is well-documented for multiple virus families[1,17,18], the mechanism(s) governing viral RNA loading into EVs has not been elucidated.

Our team discovered that mosquito-borne dengue viruses (DENV) – Flaviviridae family - secrete a subgenomic flaviviral RNA (sfRNA) inside EVs from mosquito saliva[19]. SfRNA is an RNA decay product, resulting from partial degradation of the viral RNA genome (gRNA) by 5'-3' exoribonucleases which stall on secondary structures in the 3'UTR[20]. Secondary structures include two stem loops (i.e., xrRNA1 and xrRNA2), two dumbbells (i.e., DB1 and DB2) and a final 3' stem loop (3'SL). SfRNA is abundant in salivary glands[21], which produce saliva, and is deposited via salivary EVs at the mosquito bite site[19,22]. In the bitten skin, sfRNA anti-immune properties[23] then enhance local infection and facilitate transmission[19,22], highlighting sfRNA-containing EVs as critical enhancers of pathogen dissemination. Here, we report how viral sfRNA is loaded within exosomes. We combined cell biology, molecular biology and cutting-edge genome editing using *in vitro* and *in vivo*

approaches to show that sfRNA harnesses mosquito Syntenin homolog (AeSyntenin) to induce secretion of cellular and salivary exosomes loaded with sfRNA. Our results reveal a molecular mechanism for viral RNA packaging into EVs.

Results

DENV infection stimulates EV secretion in mosquitoes

To evaluate the impact of DENV infection on EV production, we infected mosquito cells with low and high multiplicity of infection (MOI), and quantified EVs at 72 hours post-infection (hpi) (Fig. 1a). Compared to the low inoculum, the high inoculum produced higher infection intensity and quantity of secreted virions, as indicated by intracellular and extracellular gRNA copies, respectively - and higher quantity of produced and secreted sfRNA, as indicated by intracellular and extracellular sfRNA quantities, respectively (Fig. S1a-d). To determine the effect on EVs, we observed that two established mosquito EV markers, AeSyntenin and the homolog of human CD63 tetraspanin (hCD63)[3,24], increased in the cell media with infection in a dose-dependent manner (Fig. 1b-d; Fig. S2a), indicating enhanced EV marker release. In contrast, intracellular levels of these markers at the protein (Fig. 1e-g; Fig. S2b) and mRNA (Fig. S3a) levels remained unchanged. Nanoparticle tracking analysis (NTA) analysis confirmed an increase in secreted particles (Fig. 1h) and the average size (Fig. 1i) upon infection, with a uniform concentration increase across EV subpopulations (Fig. 1j,k) and higher proportions of larger EVs (Fig. 1l,m).

We examined the effect of DENV infection on EVs *in vivo* by infecting mosquitoes and analyzing tissues and saliva 10 days post infection (Fig. 1o), when infection was established and sfRNA produced in carcasses and salivary glands (Fig. S1e-h). Both AeSyntenin and hCD63 levels were elevated in infected carcasses (Fig. 1p-r; Fig. S2c), indicative of enhanced EV biogenesis, and in infected salivary glands (Fig. 1s-u; Fig. S2d),

suggesting an increased production of salivary EVs. Consistent with *in vitro* findings, *AeSyntenin* mRNA levels remained unchanged in both carcasses and salivary glands (Fig. S3b, c). Finally, we used TEM to assess EVs in saliva from infected mosquitoes (Fig. S4). Salivary EVs were mostly smaller than 40 nm (Fig. S5) and to avoid biasing EV quantification by counting virions, we did not count EVs between 40 and 60 nm. TEM analysis showed that infection increased significantly EV secretion in saliva (Fig. 1v). Together, these results indicate that DENV infection enhances salivary EV production, likely by activating secretion instead of biogenesis, as intracellular EV markers remained stable..

DENV sfRNA induces secretion of EV-packaged sfRNA

To determine whether sfRNA is required for the infection-induced EV secretion, we infected mosquito cells with a DENV infectious clone carrying deletions in the RNA pseudo-knot 1 (ΔPk1), which confers exoribonuclease resistance[25,26], to impair sfRNA biogenesis (Fig. 2a). The ΔPk1 infectious clone had a reduced sfRNA concentration, as quantified by the diminished sfRNA:gRNA ratio compared to wild-type infectious clone (Fig. 2b). Interestingly, infection with ΔPk1 reduced and abrogated the infection-induced secretion of AeSyntenin and hCD63, respectively (Fig. 2c-e; Fig. S6a). Intracellular EV marker levels remained unchanged by infection (Fig. 2f-h; Fig. S6b), consistent with prior observations upon infection. To assess whether sfRNA is sufficient to induce EV production, we transfected *in vitro*-transcribed sfRNA or a size-matched viral control RNA (Ctl. RNA) and quantified EVs 72h later (Fig. 2i). Both sfRNA and control RNA were efficiently delivered intracellularly (Fig. S7a) and were similarly reduced by half over the three day experiment duration (Fig. S7b,c). Strikingly, sfRNA transfection increased AeSyntenin secretion, with no effect on hCD63 (Fig. 2j-l; Fig. S8a), while intracellular levels of both EV markers remained unchanged (Fig. 2m-o; Fig. S8b). Although NTA analysis of ultracentrifugated EVs showed

no major change in total particle number (Fig. 2p) and mean size (Fig. 2q), size distribution analysis revealed a specific increase in the proportion of small particles (< 60 nm) following sfRNA transfection (Fig. 2r,s).

We next investigated whether transfected sfRNA is secreted inside lipid-based vesicles. We submitted sfRNA present in cell media at 72h post-transfection to a RNase resistance assay – a method previously applied to detect sfRNA packaging within EVs[19,22]. Despite multiple post-transfection washes, residual sfRNA was consistently detected in the media immediately after transfection. This may reflect rapid secretion or contamination from transfection reagents. To ensure that residual transfecting sfRNA did not bias the RNase protection evaluation for secreted sfRNA, we showed that sfRNA encapsulated in transfecting liposomes was not protected from RNase digestion (Fig. S9a). We then observed that sfRNA from transfected cell media was partially degraded by RNase, consistent with free unprotected sfRNA[19,22]. However, pre-treatment with detergent favored RNase degradation (Fig. 2t), indicating that a fraction of sfRNA was protected within lipid membranes. To test whether this packaging is specific to sfRNA, we repeated the RNase assay with Ctl. RNA, which was similarly unprotected by liposomes (Fig. S9b). In contrast to sfRNA, Ctl. RNA was similarly degraded with or without detergent (Fig. 2u), suggesting it was not vesicle-associated. Together, these results suggest that sfRNA alone is sufficient to drive the secretion of AeSyntenin-positive EVs and to be selectively packaged into EVs.

DENV sfRNA interacts with AeSyntenin

We hypothesized that sfRNA is packaged into EVs through interactions with EV-associated proteins and investigated this by performing RNA-affinity chromatography[19,27] on mosquito EV lysates (Fig. 3a). Compared to a size-matched Ctl. RNA, MS analysis identified 50 proteins that were enriched more than 1.5-fold with sfRNA, including proteins involved in EV

biogenesis and previously detected within EVs (Fig. 3b; Dataset S1). Notably, AeSyntenin was enriched with sfRNA, and its interaction with sfRNA was validated by Western blot (WB) (Fig. 3c; Fig. S10a,b). Repeating the RNA-affinity chromatography on cell lysates, we also detected the sfRNA-AeSyntenin interaction (Fig. 3d; Fig. S10c,d), suggesting that the interaction is initiated intracellularly. We further confirmed this interaction using RNA-immunoprecipitation (RIP) with anti-AeSyntenin antibody and detected sfRNA bound to AeSyntenin in both EVs from infected cells (Fig. 3f,g; Fig. S10e,f) and in DENV-infected cells (Fig. 3h,i; Fig. S10g,h). Interestingly, gRNA was also enriched in AeSyntenin RIP eluates from both EVs and cells (Fig. 3j,k). To evaluate AeSyntenin binding specificity, we measured enrichment of *AeActin*, *AeRPS7*, and *AeSyntenin* mRNAs. While all three mRNAs interacted with AeSyntenin intracellularly (Fig. S11a-c), none were recovered in RIP eluates from EVs (Fig. S11d-f), suggesting a selective EV loading mechanism. AI-based prediction of protein-RNA interactions with RoseTTAFoldNA[28] identified putative interactions between the AeSyntenin PDZ domains (aa 150-331) and the RNA stems in xrRNA1, xrRNA2 and 3' SL structures of sfRNA (Fig. S12). Collectively, these results demonstrate that DENV sfRNA binds AeSyntenin intracellularly and that this interaction persists within secreted EVs.

AeSyntenin is required for sfRNA secretion in saliva

We started by evaluating functional homology between AeSyntenin and Human Syntenin-1. Although we previously identified sequence homology in the functional PDZ domains between the two proteins[24], we assessed structural homology by using AlphaFold[29] and ScanProsite[30]. Blast between AeSyntenin and the human Syntenin-1 showed a match in the globular structure corresponding to the PDZ domains, which were predicted with high confidence (Fig. S13). We further assessed AeSyntenin functional homology by identifying interacting partners in mosquito EVs using co-immunoprecipitation (co-IP) on EVs secreted

from DENV-infected mosquito cells, for relevance to AeSyntenin's role in sfRNA loading. Among several EV-associated proteins identified (Fig. S14; Dataset S2), we detected the mosquito homolog of human ALIX, a known partner with which Syntenin induces EV biogenesis and cargo loading[9,10]. Our structural and interactome results suggest functional homology between AeSyntenin and Syntenin-1.

To assess whether AeSyntenin is required for sfRNA secretion in saliva, we silenced *AeSyntenin* in mosquitoes by injecting dsRNA, followed four days later, by intrathoracic DENV inoculation. Ten days post-infection, we quantified gRNA and sfRNA in salivary glands and saliva (Fig. 4a). While mosquito survival was unaffected at the time of inoculation, it was reduced at day 10 in the AeSyntenin-depleted, DENV-infected group (Fig. S15a,b), suggesting a fitness cost of AeSyntenin depletion upon infection. At the time of saliva collection, we confirmed AeSyntenin depletion in carcasses (Fig. 4b) and salivary glands (Fig. 4c,d). In salivary glands, AeSyntenin depletion reduced gRNA levels (Fig. 4e), suggesting a pro-viral function potentially linked to its interaction with gRNA (Fig. 3j,k). SfRNA levels were also reduced (Fig. 4f), consistent with lower gRNA template availability; however, the sfRNA:gRNA ratio remained unchanged (Fig. 4g), indicating that AeSyntenin does not influence sfRNA biogenesis. In contrast, in saliva, while gRNA levels were unaffected (Fig. 4h), sfRNA levels were significantly decreased following AeSyntenin depletion (Fig. 4i), resulting in a marked reduction in the sfRNA:gRNA ratio (Fig. 4j).

To account for the reduced salivary gland infection following AeSyntenin depletion - which could confound the analysis of sfRNA biogenesis and secretion - we repeated the experiment by compensating with a 140-fold higher viral inoculum in *AeSyntenin*-silenced mosquitoes (Fig. 4k). This approach restored infection, yielding comparable levels of gRNA, sfRNA, and sfRNA:gRNA ratios, as well as infectious particles in salivary glands (Fig. 4l-o) and whole mosquitoes (Fig. S16), irrespective of AeSyntenin status. As observed previously

(Fig. 4h), salivary gRNA levels remained unaffected (Fig. 4p), whereas salivary sfRNA levels were reduced upon AeSyntenin depletion (Fig. 4q), resulting in a significantly decreased sfRNA:gRNA ratio (Fig. 4r). Supporting a lack of AeSyntenin involvement in viral particle secretion, AeSyntenin depletion had no impact on the quantity of infectious particles in saliva (Fig. 4s). Altogether, these results demonstrate that AeSyntenin plays a key role in secretion of salivary sfRNA.

AeSyntenin in salivary glands is required for EV production and sfRNA secretion in saliva

To further investigate AeSyntenin function, we genetically abrogated its expression in mosquitoes' salivary glands. Female mosquitoes expressing Cas9 under a salivary gland-specific promoter[31] were crossed with male mosquitoes carrying multiple guide RNAs under ubiquitous promoters (Fig. 5a). We generated three female lines - each derived from a different gene insertion event and labeled with different fluorophores (i.e., RFP, EGFP and YFP) - to cross with the same male line, yielding three different progenies. Compared to the maternal Cas9 lines, AeSyntenin levels were successfully reduced in salivary glands but not in carcasses (Fig. 5b,c; Fig. S17a-e). Partial AeSyntenin deletion may result from the promoter's restricted expression to the distal lateral lobes of salivary glands[31]. TEM revealed that salivary gland-specific AeSyntenin deletion significantly lowered EV concentrations in saliva, as estimated by EV counts per image area (Fig. 5f; Fig. S18, S19a). Notably, EVs in the 30–40 nm range were selectively depleted (Fig. 5g,h; Fig. S19b,c).

To evaluate the impact of salivary gland-specific AeSyntenin deletion on sfRNA salivary secretion, we infected transgenic mosquitoes by injecting the high DENV inoculum as previously and quantified gRNA and sfRNA 10 days post-infection. Unlike systemic RNAi, tissue-specific genetic deletion of AeSyntenin did not affect survival (Fig. S20a-c),

infection or sfRNA levels in salivary glands (Fig. 5i,j; Fig. S21a,b), resulting in comparable sfRNA:gRNA ratios across Cas9 parental lines and most progeny (Fig. 5k; Fig. S21c) – with the exception of one progeny (derived from the YFP Cas9 line) which had a reduced infection and increased sfRNA:gRNA ratio (Fig. S21d-f), highlighting variability among transgenic lines. In saliva, infection levels remained unchanged in two progeny (Fig. 5l; Fig. S21h) and moderately increased in one (Fig. S21g), correlating with slightly higher salivary gland infection ($p = 0.07$; Fig. S21a). Importantly, despite progeny variation, most lines exhibited lower sfRNA levels (Fig. 5m; Fig. S21i,j) and all had reduced sfRNA:gRNA ratios (Fig. 5n-p) in saliva. Together, these findings demonstrate that AeSyntenin in salivary glands specifically contributes to EV-associated sfRNA secretion in saliva.

Discussion

Our study elucidates the first mechanism for selective loading and secretion of viral RNA into exosomes. First, we demonstrate that infection-induced secretion of salivary EVs is partially dependent on the production of sfRNA. Second, we confirm that sfRNA actively promotes EV secretion by showing that sfRNA alone is sufficient to drive its own packaging into small EVs. Third, we provide evidence that sfRNA binds both intracellularly and extracellularly to AeSyntenin, which we identified as a key mediator of small EV production in mosquito saliva. Finally, we establish that AeSyntenin in salivary glands is required for the secretion of sfRNA-containing exosomes in saliva. Collectively, these findings support a model in which sfRNA interacts with AeSyntenin to mediate its loading into exosomes, inducing their secretion in mosquito saliva.

Although mechanisms underlying viral RNA loading into EVs remain poorly defined, several pathways have been proposed for the selective incorporation of host RNA into EVs[32,33]. One well-supported model involves RNA-binding proteins (RBPs) that recognize

specific RNA motifs and subsequently interact with EV biogenesis proteins to mediate cargo sorting[34,35]. The involvement of RBPs is supported by the detection of multiple RBPs within EVs, along with the enrichment of their inferred RNA targets. For example, hnRNPA2B1, which contains four RNA-binding domains,[36] and the La protein[37] have been shown to bind specific microRNAs and facilitate their inclusion into EVs. In addition, ALG-2-interacting protein X (ALIX)—a key regulator of EV biogenesis—interacts with RBPs such as Dicer-2 to control the selective loading of miRNAs[38]. Alternatively, direct electrostatic interactions between RNA and membrane lipids[39] or indirect interactions through lipid-binding RBPs[40] can drive RNA incorporation within EV membranes. In this study, we demonstrate that the interaction between sfRNA and AeSyntenin - a key player in EV biogenesis - drives sfRNA secretion into EVs. Based on the small size of AeSyntenin-dependent EVs and the homology with human Syntenin-1[9], we suggest that the sfRNA-containing EVs are exosomes. While our previous work identified sfRNA-interacting RBPs using mosquito cell lysates[19], the AeSyntenin co-IP did not yield RBPs in the current study. This suggests that AeSyntenin-mediated loading of sfRNA into EVs occurs independently of RBPs. Supported by the capacity of Syntenin-1 to load host and viral proteins into exosomes[41,42], our results show that viral RNA harnesses EV biogenesis proteins for secretion.

Overall, we used mosquito vectors and a global viral pathogen as models to delineate the first mechanism of viral RNA loading into exosomes. Leveraging homology in EV biogenesis, this knowledge could help understand how other viruses exploit EVs in multiple animals.

Limitations of the study

We leveraged our expertise in mosquito-borne viral diseases to study EV loading. However, our study system suffers from several technical limitations. The nanoliter-size volumes of

mosquito saliva preclude the use of biochemical methods usually applied for EV isolation. Additionally, although we generated and previously characterized[24] a mosquito-specific antibody against EV markers, we did not have access to multiple EV-targeted antibodies, reducing our capacity to characterize mosquito EVs. Moreover, sfRNA sequence identity with gRNA did not allow its direct quantification, and instead we relied on a well-supported[19,21,22] indirect subtractive sfRNA quantification.

Acknowledgements

We are grateful to the VectoPole team in Montpellier, particularly Bethsabée Scheid and Carole Ginibre for providing mosquito eggs. We thank Sarah Debaveye for help with generating virus constructs. The authors acknowledge the ISO 9001 certified IRD i-trop HPC (member of the South Green Platform) at IRD Montpellier for providing HPC resources that have contributed to the research results reported within this paper. URL: https://bioinfo.ird.fr/- http://www.southgreen.fr.

Disclosure and competing interests statement

The authors declare that they have no conflict of interest.

Funding

PhD scholarship for FR was provided by the French ministry of research and higher education (CBS2 doctoral school) on a competitive basis. Support for this research came from French Agence Nationale pour la Recherche (ANR-20-CE15-0006) and EU HORIZON-HLTH-2023-DISEASE-03-18 (#101137006) to JP, from the Research Foundation Flanders (FWO) under the Excellence of Science (EOS) program (no. 30981113; VirEOS) and the EU RIA Health Action (no. 101137459; Yellow4FLAVI) to KD.

Material and methods

Cells and viruses. *Aedes aegypti* Aag2 and *Aedes albopictus* C6/36 (ATCC - CRL1660) were grown in Roswell Park Memorial Institute (RPMI) medium (Gibco) and Dulbecco's Modified Eagle Medium (DMEM) (Gibco), respectively, with 10% heat-inactivated fetal bovine serum (FBS) (Gibco), 1X non-essential amino acids (Gibco), and 1% penicillin/streptomycin (Gibco) at 28°C with 5% CO_2. Hamster kidney BHK-21 cells (ATCC – CL10) were grown in RPMI medium with 5% heat-inactivated FBS and 1% penicillin/streptomycin at 37°C, 5% CO_2.

DENV-2 New Guinea C strain (NGC) was obtained from ATCC (VR-1584). Yellow fluorescent protein (mCitrine)-tagged NGC DENV2-ΔPK1 mutant reporter virus was generated using standard molecular biology techniques, i.e. side-directed PCR mutagenesis (KapaHF HotStart ReadyMix, Roche) and homologous recombination in yeast[43], to modify infectious molecular clone pShuttle-DV2/mCherry[44]. To abolish sfRNA expression, a three-nt base exchange was introduced in the DENV2 3'-UTR cDNA impairing the intramolecular base-paring between the top of stem-loop (SL II) and its proximal downstream RNA required for the formation of pseudoknot structure 1 (pk1)[20]. Recombinant virus was rescued by plasmid DNA transfection of BHK21 cells using TransIT-LT1 transfection reagent (MirusBio), amplified by passage in C6/36 mosquito cells and quantified by plaque titration as previously described[43]. Wild-type NGC infectious clone were similarly produced with mCherry sequence at the same position as mCitrine.

Mosquitoes. *Aedes aegypti* mosquitoes from the Bora Bora colony[45] were maintained in BugDorm cages (BugDorm) at 27 ± 1°C, with 70 ± 5% relative humidity, under a 12 h:12 h

light:dark cycle, and provided with *ad libitum* access to a 10% sucrose solution. Larvae were reared at 28°C in Milli-Q water supplemented with fish food flakes (TetraMin) until pupation.

Cell infection. For IP, 1.8 x 10^7 Aag2 cells were incubated with DENV at a MOI of 1 in 5 ml of FBS-free cell media for 1 h. For WB and RT-qPCR analyses, 2.5 x 10^5 Aag2 cells were incubated with DENV at a MOI of 0.05 or 1 in 150 µl of FBS-free cell media for 1 h. For NTA, 8 x 10^6 Aag2 cells were incubated with DENV at a MOI of 0.05 or 1 for 1 h in 2 ml of FBS-free cell media for 1 h. After removing the inoculum, cells were incubated with complete media containing 2% EV-free FBS for 72 h.

Quantification of gRNA, sfRNA and Ctl RNA. Total RNA was extracted using E.Z.N.A. Total RNA Kit I and eluted in DEPC-treated water. gRNA, wild-type sfRNA/3'UTR, Pk1 mutated sfRNA/3'UTR and Ctl RNA were quantified by RT-qPCR using the iTaq SYBR GREEN One-Step Kit (Bio-Rad) with primers detailed in Table S1. A total reaction volume of 10 µl containing 0.3 µl of 300 nM of forward primer, 0.3 µl of 300 nM reverse primer, 5 µl of iScript master mix, 2.275 µl of water nuclease-free water and 2 µl of RNA extract was amplified using LightCycler 96 (Roche) with the following thermal profile: 50°C for 15 min, 95°C for 1 min, followed by 40 cycles of 95°C for 10 sec and 60°C for 15 sec, with a final melting curve analysis.

Absolute quantification was achieved by amplifying the qPCR templates using forward T7-tagged primers detailed in table S1. Templates were transcribed using the MegaScript T7 Kit and purified with the E.Z.N.A. Total RNA Extraction Kit I. RNA concentrations were measured using a NanoDrop spectrophotometer (Thermo Fisher Scientific) and serial dilutions were used to generate absolute standard curves.

SfRNA copies were calculated by subtracting gRNA copies (quantified using primers targeting the envelop) from the combined sfRNA and 3'UTR copy numbers (quantified using sfRNA/3'UTR primers), as previously developed[21]. For samples containing detectable levels of sfRNA, sfRNA:gRNA ratio was calculated by dividing sfRNA to gRNA copy numbers.

Western Blot (WB). WB analyses were conducted on eluates from RNA affinity chromatography and IP, and on lysates from Aag2 cells, cell media, whole mosquitoes and salivary glands. Cell lysate was obtained by adding RIPA buffer IV (Bio Basic), centrifugating the lysate at 20,000 × g for 20 min and collecting the supernatant. Cell media was pre-cleared by centrifugation at 3,500 x g for 10 min and lysed in RIPA buffer IV. Mosquito and salivary gland lysates were obtained by homogenizing 5 carcasses and 10 salivary glands in 250 or 150 µl of RIPA buffer IV, respectively, with silica beads (BioSpec) using a BeadBeater homogenizer (MP Biomedicals) and collecting supernatants after centrifugation at 14,000 rpm for 10 min at 4°C. Proteins from eluates and lysates were quantified using Qubit protein assay (ThermoFisherScientific). Homogenized quantities of proteins were diluted in reducing Laemmli SDS buffer, heated to 95°C for 10 min, separated on NuPAGE 4-12% acrylamide gel (Invitrogen) and transferred onto a 0.2 µm nitrocellulose membrane (Bio-Rad) using Trans-Blot turbo Transfer System (Bio-Rad). Membranes were washed with 0.1% Tween 20 in PBS, blocked with 5% milk (Régilait) for 1 h at RT, incubated overnight at 4°C with primary antibodies diluted in 0.1% Tween 20 in PBS. Antibodies included 1:500 rabbit anti-human CD63 (Ab134045,clone EPR5702, Abcam), 1:500 mouse anti-human pan-actin (MA5-11869, clone ACTN05, Thermo Scientific), and 1:500 rabbit custom-made anti-AeSyntenin[46]. Secondary antibody staining was performed with 1:2,000 HRP-conjugated anti-rabbit IgG (7074, Cell Signaling Technology) or 1:2,000 HRP-conjugated anti-mouse IgG (7076, Cell Signaling Technology) in 0.1% Tween 20 5%

milk in PBS for 1 h at RT. Blots were revealed with SuperSignal West Pico PLUS Chemiluminescent Substrate (Thermo Scientific) or SuperSignal West Femto Chemiluminescent Substrate (Thermo Scientific) using a ChemiDoc MP Imaging System (Bio-Rad) and analyzed with ImageLab Software (Bio-Rad). Blot intensity was estimated with ImageLab and normalized to actin level.

Nanoparticle Tracking Assay (NTA). Cell media was diluted by half in PBS and analyzed using a NanoSight NS300 instrument (Malvern) equipped with a 488 nm laser. The capture settings were as follows: camera type sCMOS, laser type Blue488, camera level 12, slider shutter 1206, slider gain 366, frame rate (FPS) 25.0, number of frames 1498, temperature 25.0 °C, viscosity 0.9 cP (for water), and syringe pump speed 40. Five 1-minute videos were recorded, and particle analysis was conducted using NanoSight NTA software version 3.4 (build 3.4.4, Malvern). NTA analyses were performed at the Charles Gerhardt Institute, Montpellier, France.

Infection of mosquitoes. Three-to-five day-old female mosquitoes were intrathoracically microinjected with 5 FFU of wild-type DENV in a single injection of 69 nl using Nanoject II (Drummond). An equivalent volume of RPMI was injected as control. DsRNA-injected female mosquitoes were microinjected with 5 or 700 FFU of wild-type DENV at 4 days post dsRNA injection. Mosquitoes were maintained on a 10% sugar solution for an additional 10 days before analysis.

Extracellular vesicle (EV) isolation. EV-free FBS was produced by ultracentrifugating heat-inactivated FBS at 100,000 × g for 18 h using an S58-A rotor (k-factor 50, Thermo Scientific) in a Sorvall MX Plus Series Floor Model Micro-Ultracentrifuge (Thermo Scientific). EV-free

FBS was collected by leaving approximately 1 ml of residual volume at the bottom of the 8 ml tube, filtered through a 0.22 µm filter (Sartorius), and stored at 4°C. 1.8 x 10^6 Aag2 cells per T175 flask were maintained in complete medium supplemented with 2% EV-free FBS for 3 days. Cell media was then centrifugated at 3,500 × g for 5 min to remove cell debris. The clarified supernatant was ultracentrifugated at 100,000 × g for 3 h to obtain an EV-concentrated pellet. For NTA, the EV-concentrated pellet was washed in PBS and ultracentrifugated one more time at 100,000 x g for 3h before resuspension in PBS.

Collection of mosquito saliva and tissues. Mosquitoes were starved for 24h, cold-anesthetized, and immobilized by removing their wings and legs. The proboscis of each mosquito was individually inserted into a 20 µl pipette tip containing 10 µl of pre-warmed DMEM supplemented with 0.5 mM ATP (Invitrogen) and 1% Erioglaucine (25 mM, Sigma-Aldrich) for 1 h[22]. Mosquitoes with blue-colored abdomens, indicating ingestion of the dye, were considered as having salivated. For TEM observation, saliva was collected in bulk. Hundreds of mosquitoes were let to feed on artificial feeding system (Hemotek) containing 3 ml of DMEM supplemented with 0.5 mM ATP and 1% Erioglaucine covered with a silicone membrane for 2 h. The DMEM media was then precleared by centrifugation at 1,500 g for 10 min at 4°C, ultracentrifugated at 100,000 g for 3 h at 4°C and resuspended in 30 µl of PBS. Number of salivating mosquitoes was estimated by counting the number of blue-abdomen mosquitoes, indicating salivation and quantities of EVs were normalized per mosquitoes between infected and non-infected samples. For RNA quantification, individual saliva samples were transferred into 200 µl of TRK lysis buffer. For FFU assays, pooled saliva samples from 10 mosquitoes was combined with 100 µl of RPMI medium supplemented with 1% P/S and 1% antibiotic-antimycotic solution (Gibco). Following saliva collection, salivary glands were dissected using fine forceps. For RNA quantification, 5

salivary glands were pooled in 200 µl of TRK lysis buffer. For FFU assays, 5 salivary glands were pooled in 150 µl of RPMI 1% P/S and 1% antibiotic-antimycotic. For WB, 5 or 10 salivary glands were pooled in 150 µl of RIPA buffer IV. Remaining carcasses were collected and processed similarly by pools of five. Tissues and saliva samples were homogenized using silica beads with a BeadBeater homogenizer. RNA was extracted using the EZNA Total RNA Kit I. For FFU assays, homogenized tissues and saliva were sterilized by filtration through a 0.22 µm filter (Millex-GV). For WB, lysates from salivary glands and carcasses were pre-cleared by centrifugation at 3,500 × g for 10 min.

Transmission electron microscopy (TEM). For uninfected and infected EV saliva, 3 µl of ultracentrifugated EV solution was absorbed on a glow-discharged 300 mesh formvar carbon-coated grid (Electron Microscopy Science) and stained with 1% uranyl acetate in two steps. Grids were observed using a JEOL 1400 Flash transmission electron microscope at 120kV. Micrographs were recorded using a One View camera (Gatan Inc.). Experiment was performed at the Center of Structural Biology of Montpellier, CNRS, France. For EV saliva from transgenic mosquitoes, 7 µl of ultracentrifugated salivary EV solution was loaded onto a formvar-coated copper grid 100 mesh (EMS FCF100-Cu-50), left to settle for 2 min, and dried with a blotting paper. The grid was stained with 1% uranyl acetate and analyzed using a TEMF20 operating at 120 KV (Tecnai) with a Veleta numeric camera (Olympus) at the Neuroscience institute of Montpellier, INSERM U1298, France.

Production of sfRNA and control RNA (Ctl RNA). sfRNA and Ctl RNA, corresponding to a DENV NS2 fragment[27], were amplified from viral cDNA using T7 promoter-tagged forward primers. sfRNA and Ctl. RNA primers are detailed in table S1. PCR products were size-validated by agarose gel electrophoresis, purified using the QIAquick PCR Purification

Kit, and *in vitro* transcribed using MEGAscript T7 Kit. Transcripts were purified with the E.Z.N.A. Total RNA Kit I and quantified via NanoDrop. RNA fragments were treated with RNA 5' polyphosphatase (Biosearch Technologies), and re-purified and quantified as above. Samples were incubated at 95 °C for 5 min and gradually cooled to 4 °C for folding.

Transfection of sfRNA and Ctl RNA. 10^{11} and 10^{12} copies of monophosphorylated folded sfRNA and Ctl RNA, respectively, were transfected for 1 h using TransIT mRNA Transfection Kit (Euromedex) into 2.5 x 10^5 Aag2 cells for WB analysis or into 1.2 x 10^6 Aag2 cells for 1 h for NTA analysis. Difference between sfRNA and Ctl RNA amounts was to compensate for a lower transfection efficiency of Ctl RNA (Fig. S7a). Transfection media was removed and cells were washed three times with pre-warmed RPMI medium. After three days of incubation with 2% EV-free FBS 1% P/S 1X NEAA RPMI, media was collected, pre-cleared by centrifugation at 3,500 x g for 10 min and lysed in RIPA buffer IV. For NTA analysis, pre-cleared cell media was ultracentrifugated at 100,000 × g for 3 h, the pellet washed, ultracentrifugated at 100,000 x g for 3 h, and resuspended in 500 µl PBS. Aag2 cells were lysed in TRK lysis buffer (EZNA Total RNA Kit I) for RNA quantification or in 100 µl of RIPA buffer IV for WB.

RNAse resistance assay. Three days post sfRNA and Ctl RNA transfection, 1 ml of cell media was pre-cleared at 3,500 x g for 10 min, divided into equal volumes of 4 x 200 µl and treated with different conditions. Samples were treated with 2.5 µl of 0.1 % triton X 100 (Sigma or PBS as control and incubated at 4°C at 30 min. Then, 5 µl of RNase A/T1 (Thermofisher Scientific) or PBS as control was added and samples were incubated at 37°C for 30 min before RNA extraction using E.Z.N.A. Total RNA extraction Kit I.

RNA affinity chromatography. RNA affinity chromatography was performed as previously described[27] with minor modifications. 1 ml of NHS Mag Sepharose bead (Cytiva) flurry was washed four times with 1 ml of 1 mM HCl (Carlo Erba) and incubated in 950 µl of coupling buffer [0.2 M $NaHCO_3$ (Sigma), 0.5 M NaCl (Sigma), pH 8.3] with 50 µl of 5 mM tobramycin (Sigma) overnight at 4°C under gentle rotation. Tobramycin beads were blocked in 1 ml of blocking buffer [20 mM Tris pH 7.0 (Sigma), 1 mM $CaCl_2$ (Sigma), 1 mM $MgCl_2$ (Sigma), 300 mM KCl (Sigma), 0.1 mg/ml of tRNA (Ambion), 0.5 mg/ml BSA (Sigma), 0.2 mM Dithiothreitol (Biorad), 0.01% NP-40 (MP Biomedical)] for 1 h at 4°C, washed three times with PBS and resuspended in 500 µl of PBS. DENV sfRNA and a same-size control RNA fragment both flanked by a tobramycin aptamer sequence were amplified from plasmids[27,47] using T7-tagged forward primers detailed in table S1. After size validation on agarose gel, PCR products were purified using the QIAquick PCR Purification Kit (Qiagen) and transcribed using MEGAscript T7 Kit (Thermo Fisher). Transcribed RNA was extracted with EZNA Total RNA Kit I (Omega) and quantified using Nanodrop. 30 µg of *in vitro*-transcribed sfRNA or control RNA in 200 µl of RNA binding buffer (20 mM Tris pH 7.0, 1 mM $CaCl_2$, 1 mM $MgCl_2$, 75 mM NaCl, 145 mM KCl, 0.1 mg/ml yeast tRNA, 0.2 mM Dithiothreitol) was heated to 95°C for 5 min and slowly cooled to RT to enable RNA folding. The RNA solution was incubated with 30 µl of tobramycin-coupled beads for 1 h at 4°C under end-over-end rotation. Beads were washed once with 250 µl of RNA washing buffer (20 mM Tris pH 7.0, 1 mM $CaCl_2$, 1 mM $MgCl_2$, 75 mM NaCl, 145 mM KCl, 0.1% NP-40, 0.2 mM Dithiothreitol).

1.8×10^7 uninfected Aag2 cells or isolated EVs were lysed in 1 ml and 500 µl of lysis buffer [50 mM Tris pH 7.5 (Sigma), 150 mM NaCl, 1% NP-40, 1 X protease and phosphatase inhibitor (Sigma)], respectively. 417 µl of cell lysate in 500 µl of 1 X modified protein buffer (2 mM $CaCl_2$, 2 mM $MgCl_2$, 290 mM KCl, 4 mM Dithiothreitol) or 210 µl of EV lysate in

300 µl of 1 X modified protein buffer were pre-cleared with 30 µl of tobramycin bead flurry during 1 h at 4 °C and then incubated with beads from 30 µl of RNA-bead flurry for 2 h at 4°C with end-over-end rotation. Beads were washed four times in 500 µl of 145 mM protein washing buffer (20 mM Tris pH 7.0, 1 mM $CaCl_2$, 1 mM $MgCl_2$, 75 mM NaCl, 145 mM KCl, 0.5% NP-40). Elution for MS analysis was performed by incubating beads in 20 µl of elution buffer (20 mM Tris pH 7.0, 1 mM $CaCl_2$, 3 mM $MgCl_2$, 145 mM KCl, 5 mM tobramycin, 0.2 mM Dithiothreitol) for 5 min on ice and elution for WB analyses was performed in 25 µl of Laemmli SDS buffer (Thermo Scientific) and heated to 95 °C for 5 min.

Mass spectrometry (MS). Eluates from RNA affinity chromatography were analyzed at the PPM laboratory (Pôle Protéome de Montpellier, France). Briefly, peptide samples were reconstituted in 10 µl of buffer A (0.1% formic acid) and injected into nano-flow HPLC system (Ultimate 3000 RSLC, Thermo Fisher Scientific) coupled to a mass spectrometer equipped with a nanospray source (Q-Exactive HF, Thermo Fisher Scientific). Peptides were separated on a capillary column (0.075 mm × 500 mm, Acclaim PepMap 100, reverse-phase C18, NanoViper, Thermo Fisher Scientific) using a gradient of 2-40% B over 120 minutes with A = 0.1% formic acid and B = 0.1% formic acid in 80% acetonitrile, at a flow rate of 300 nl/min (total runtime: 150 min). Spectra were recorded using Xcalibur 4.1 software (Thermo Fisher Scientific) with the method file 120LowQtt.meth. Spectral data were analyzed with MaxQuant v1.6.10.43, including the script leading FPP v3.2. The following databases were used: RefProteome_Aedes_aegypti-cano_2021_01_UP000008820_7159.fasta, Uniprot_SPOFR_2020_02.fasta, VectorBase-52_AaegyptiLVP_AGWG_AnnotatedProteins.fasta, and contaminants_fpp_180320.fasta. Data validation was performed using a 1% FDR filter at both peptide and protein levels. Proteins with more than 1.5 fold enrichment with LFQ ratio and 2 fold enrichment with

MS/MS pseudoRatio were considered significantly enriched. The mass spectrometry proteomics data have been deposited to the ProteomeXchange Consortium via the PRIDE[48] partner repository with the dataset identifier PXD065152. (Username: reviewer_pxd065152@ebi.ac.uk , Password: jQGpLX9honIs).

Eluates from AeSyntenin co-IP were analyzed by the Proteomic Platform of Strasbourg-Esplanade (PPSE) at the Institut de Biologie Moléculaire et Cellulaire (IBMC). Briefly, proteins were first precipitated overnight using 0.1 M ammonium acetate in 100% methanol. After centrifugation at 12,000g and 4°C for 15 min, the pellets were washed twice with 0.1 M ammonium acetate in 80% methanol. This precipitation step was repeated once more. Then, proteins were dried using a Speed-Vac concentrator. The dried pellets were resuspended in 100 µL of 50 mM ammonium bicarbonate, reduced with 5 mM dithiothreitol at 95°C for 10 minutes, and alkylated with 10 mM iodoacetamide at room temperature for 30 min in the dark. Samples were digested with 150 ng sequencing-grade trypsin (Promega) at 37°C overnight. Peptides were resuspended in 0.1% formic acid, and 3/64 of the sample was loaded for nLC-MS/MS analysis. Samples were analyzed using a timsTOF Pro 2 coupled with a NanoElute 2 (Bruker Daltonik GmbH) in Data-Independent Acquisition and Parallel Accumulation Serial Fragmentation (DIA-PASEF) mode. Peptides were separated on an IonOpticks Aurora Elite column (25 cm × 75 µm, 1.7 µm particle size, and 120 Å pore size; AUR3–15075C18-CSI) with a 45-minute elution gradient. Data were searched against the *Aedes aegypti* database from UniProt (v2021_03, 33 998 sequences) using DIANN 1.9 software with a library-free approach keeping most of the default parameters. One missed cleavage and one variable modification were allowed (M-Ox, Ac-Nterm), and match between runs was enabled. Prostar software (1.34.5) was used for statistical analyses. Imputation of missing values was based on the 1% detection quantile, and a LIMMA statistical test was

used for each comparison. The mass spectrometry proteomics data from the immunoprecipitations have been deposited to the ProteomeXchange Consortium via the PRIDE partner repository with the dataset identifier PXD065851 (Username: reviewer_pxd065851@ebi.ac.uk , Password: GmeflV8jgwL9).

Immunoprecipitation (IP) and co-immunoprecipitation (co-IP). Infected Aag2 cells and EVs from infected Aag2 cells were lysed in 500 µl of NT2 buffer [200 mM KCl, 20 mM HEPES pH 7.2, 2% N-dodecyl-β-D-maltoside (Thermofisher Scientific), 1% Igepal (Sigma), 100 U/mL Murine RNase inhibitor (Biolabs)] and supernatant was collected after centrifugation at 13,000 × g for 13 min at 4°C. 100 µl of SureBeads Protein G Magnetic Beads (Bio-Rad) were washed with 500 µl of 0.01% Tween 20 in PBS, blocked with 50 µl of 1% BSA 0.01% Tween 20 in PBS for 10 min at 4°C, washed with PBS and incubated for 1 h at 4°C with 500 µl of 0.01% Tween 20 in PBS containing 2.5 µg of custom-made anti-AeSyntenin antibody[46] on a disk rotator. Beads were similarly incubated with anti-rabbit IgG antibody (Invitrogen) as control. After three washes with 500 µl of 0.01% Tween 20 in PBS, beads were incubated with homogenized volumes of lysed proteins for 2 h at 4°C on a rotator. 1 % of initial input was kept for analysis by WB as control. After washes, beads diluted in 500 µl of 0.01% Tween 20 in PBS were separated into aliquots of 100 µl for WB analysis and 400 µl for RNA quantification. WB samples were resuspended in 30 µl of Laemmli SDS buffer and warmed at 95°C for 5 min. RNA quantification samples were resuspended in 350 µl of TRK lysis buffer before extraction with EZNA Total RNA extraction Kit I. For co-IP, all beads were resuspended in 50 µl of Laemmli SDS buffer and heated at 95°C for 5 min. Elution was repeated once with 50 µl of Laemmli SDS buffer to obtain a final elution volume of 100 µl.

Affinity of the anti-AeSyntenin antibody for sfRNA was assessed by coupling SureBeads Protein G Magnetic Beads with either anti-rabbit IgG or rabbit anti-AeSyntenin antibody as above and incubating them with 10^{1} copies of *in vitro*-transcribed sfRNA for 2 h at 4 °C on a disk rotator. Elution for RNA extraction was performed as above.

RoseTTAFold2NA prediction. Interaction predictions between the 3D structures of xrRNA1, xrRNA2, xrRNA1-2, SL1-SL2, DB1, DB2, 3'SL and the AeSyntenin was performed on RoseTTAFold2NA version 0.2[49]. Molecular visualization was performed with Molstar[50].

Quantification of mRNA. Total RNA was extracted using the EZNA Total RNA Kit I, cleared of genomic DNA using DNAse following protocol from gDNA Clear cDNA Synthesis kit (Biorad), quantified with a NanoDrop, normalized, and reverse transcribed using iScript gDNA Clear cDNA Synthesis Kit (Bio-Rad). *AeSyntenin* mRNA was quantified in a total reaction of 10 µl, containing 2 µl of Hot FirePol SolisGreen qPCR mix (Euromedex), 0.3 µl of 300 nM forward, 0.3 µl of 300 nM reverse primers (Table S1), 5.4 µl of nuclease-free water and 2 µl of cDNA. qPCR thermal profile consisted of 95°C for 5 min, followed by 40 cycles of 95°C for 15 sec, 60°C for 20 sec, and 72°C for 20 sec, with a final melting curve analysis on a LightCycler 96 (Roche). *Actin* and *RPS7* mRNA were quantified as housekeeping genes and the geometric mean of their Ct values was used for normalization using the delta-delta Ct method.

RNAi-mediated silencing. Target sequences were amplified from Aag2 cDNA using GoTaq Master Mix (Promega) and 400 nM T7-flanked primer pairs (Table S1) designed via the E-RNAi website[51] with the following thermal profile: 95°C for 5 min; 45 cycles of 95°C for 15

sec., 55°C for 15 sec., and 72°C for 45 sec.; 72°C for 10 min. After product size confirmation on agarose gel, PCR products were purified using the QIAquick PCR Purification Kit and transcribed overnight with the MEGAscript T7 Kit. RNA was extracted with the EZNA Total RNA Kit I, adjusted to 14 µg/µl, and annealed by heating at 95°C for 5 min followed by gradual cooling. Negative control dsRNA targeting LacZ[52] was similarly produced (Table S1). Four-day-old female mosquitoes were cold-anesthetized and injected with 138 nl of dsRNA using Nanoject II microinjector (Drummond Scientific). Mosquitoes were maintained on a 10 % sugar solution.

Focus forming unit (FFU) assay. Samples were subjected to a four-fold serial dilution in RPMI medium and 150 µl of each dilution was incubated with 1.5×10^5 BHK-21 cells for 1 h on a rocking platform. After removing the inoculum, cells were overlaid with 500 µl of 1% carboxymethyl cellulose (CMC) (Sigma) in 2% FBS (Gibco) RPMI medium. After 5 days, cells were fixed with 4% paraformaldehyde (VWR) in PBS, permeabilized with 0.3% Triton X-100 (Euromedex), blocked with 1% FBS in PBS, and stained using a 1:200 mouse monoclonal anti-envelope antibody (4G2, provided by Dr Subhash Vasudevan, Duke-NUS Medical School, Singapore) and 1:500 secondary anti-mouse IgG Alexa Fluor 488 (Invitrogen). FFU were counted using the EVOS m5000 microscope (Invitrogen) in three replicates per dilution, and average FFU per sample was calculated per ml.

Salivary gland-specific abrogation of AeSyntenin. Golden Gate Cloning was used to construct a first piggyBac transgenesis vector with Cas9 under the control of the 30Ka promoter[31]. In a second piggyBac transgenesis vector, different guide RNAs targeting *AeSyntenin* were placed under the control of four different U6 promoters: protospacer GACGAGTCCTTAACGATGG(CGG) under control of U6 promoter AAEL017774;

GTCACCAACGGAATTCGAG(AGG) under U6 AAEL017763; GATACTTCCGGTTGGTAAG(CGG) under U6 AAEL017774, and GGGATTGGAGCTCAGCCGTG(AGG) under U6 AAEL017702. The sequences of the transgenesis plasmids are provided in Fig. S22 and DataSet S3 and S4. Transgenic mosquitoes were obtained by injecting embryos of the Liverpool strain with 240 ng/l of piggyBac plasmid mixed with 80 ng/µl of transposase helper plasmid[53]. Injected mosquitoes reaching adulthood and showing transient expression of the fluorescence marker were backcrossed to wild-types. In the next generation (G1), transgenic larvae were selected based on expression of the plasmid's fluorescence markers[54]. Single G1 females were crossed to wild-type males. Transgenes showing about 50% inheritance, indicative of probable single insertions, were retained and the G2 positives of each progeny were self-crossed to establish lines. In the G3 generation, homozygous larvae were selected by their stronger fluorescence to establish stable lines. Three lines with Cas9 expression were produced each with a different selection fluorescent marker (i.e., RFP, EGFP, YFP), while one line with gRNA was produced. From the guide RNA lines, seven homozygous males were mass-crossed with twenty virgin Cas9-expressing females. The resulting eggs were allowed to develop for 3 to 5 days before hatching. Individual containers were provided with blood meals. Blood-fed females were then transferred to separate boxes for oviposition. After egg-laying, the egg papers were removed, and the eggs were allowed to mature for at least five days before hatching the cohorts selected for experiments.

Statistics. One-tailed T-test was applied to test differences in log-transformed gRNA, sfRNA copy numbers and fold changes, in non-transformed sfRNA:gRNA ratio, AeSyntenin and hCD63 protein quantities. Variations in concentration and proportion of particles by size were tested using X^2 test. Differences in RNA quantities after RNase assay and in AeSyntenin and

hCD63 protein quantities upon different infection MOI were assessed with Fisher's LSD multiple comparison test. Statistical analyses were conducted using Prism v8 (GraphPad).

References

1. Rey-Cadilhac, F., Rachenne, F., Missé, D. & Pompon, J. Viral Components Trafficking with(in) Extracellular Vesicles. *Viruses* **15**, 2333 (2023).
2. Zhu, X., Lin, X., Hu, L., Wang, L. & Zhu, Q. Harnessing crosstalk between extracellular vesicles and viruses for disease diagnostics and therapeutics. *Extracell Vesicles Circ Nucleic Acids* **5**, 458–60 (2024).
3. Théry, C. *et al.* Minimal information for studies of extracellular vesicles 2018 (MISEV2018): a position statement of the International Society for Extracellular Vesicles and update of the MISEV2014 guidelines. *Journal of Extracellular Vesicles* **7**, 1535750 (2018).
4. Couch, Y. *et al.* A brief history of nearly EV erything – The rise and rise of extracellular vesicles. *J of Extracellular Vesicle* **10**, e12144 (2021).
5. Jadli, A. S., Ballasy, N., Edalat, P. & Patel, V. B. Inside(sight) of tiny communicator: exosome biogenesis, secretion, and uptake. *Mol Cell Biochem* **467**, 77–94 (2020).
6. Zhang, Y., Liu, Y., Liu, H. & Tang, W. H. Exosomes: biogenesis, biologic function and clinical potential. *Cell Biosci* **9**, 19 (2019).
7. Van Niel, G., D'Angelo, G. & Raposo, G. Shedding light on the cell biology of extracellular vesicles. *Nat Rev Mol Cell Biol* **19**, 213–228 (2018).
8. Zimmermann, P. *et al.* Characterization of Syntenin, a Syndecan-binding PDZ Protein, as a Component of Cell Adhesion Sites and Microfilaments. *MBoC* **12**, 339–350 (2001).
9. Baietti, M. F. *et al.* Syndecan–syntenin–ALIX regulates the biogenesis of exosomes. *Nat Cell Biol* **14**, 677–685 (2012).
10. Ghossoub, R. *et al.* Syntenin-ALIX exosome biogenesis and budding into multivesicular bodies are controlled by ARF6 and PLD2. *Nat Commun* **5**, 3477 (2014).

11. Friand, V., David, G. & Zimmermann, P. Syntenin and syndecan in the biogenesis of exosomes: Syndecan-syntenin pathway in exosome biogenesis. *Biol. Cell* **107**, 331–341 (2015).

12. Van Niel, G., D'Angelo, G. & Raposo, G. Shedding light on the cell biology of extracellular vesicles. *Nat Rev Mol Cell Biol* **19**, 213–228 (2018).

13. Valadi, H. *et al.* Exosome-mediated transfer of mRNAs and microRNAs is a novel mechanism of genetic exchange between cells. *Nat Cell Biol* **9**, 654–659 (2007).

14. Mittelbrunn, M. *et al.* Unidirectional transfer of microRNA-loaded exosomes from T cells to antigen-presenting cells. *Nat Commun* **2**, 282 (2011).

15. Pegtel, D. M. *et al.* Functional delivery of viral miRNAs via exosomes. *Proc. Natl. Acad. Sci. U.S.A.* **107**, 6328–6333 (2010).

16. Zomer, A. *et al.* In Vivo Imaging Reveals Extracellular Vesicle-Mediated Phenocopying of Metastatic Behavior. *Cell* **161**, 1046–1057 (2015).

17. Bukong, T. N., Momen-Heravi, F., Kodys, K., Bala, S. & Szabo, G. Exosomes from Hepatitis C Infected Patients Transmit HCV Infection and Contain Replication Competent Viral RNA in Complex with Ago2-miR122-HSP90. *PLoS Pathog* **10**, e1004424 (2014).

18. Caobi, A., Nair, M. & Raymond, A. D. Extracellular Vesicles in the Pathogenesis of Viral Infections in Humans. *Viruses* **12**, 1200 (2020).

19. Yeh, S.-C. *et al.* The anti-immune dengue subgenomic flaviviral RNA is present in vesicles in mosquito saliva and is associated with increased infectivity. *PLoS Pathog* **19**, e1011224 (2023).

20. Pijlman, G. P. *et al.* A Highly Structured, Nuclease-Resistant, Noncoding RNA Produced by Flaviviruses Is Required for Pathogenicity. *Cell Host & Microbe* **4**, 579–591 (2008).

21. Pompon, J. *et al.* Dengue subgenomic flaviviral RNA disrupts immunity in mosquito salivary glands to increase virus transmission. *PLoS Pathog* **13**, e1006535 (2017).

22. Serrato-Pomar, I. *et al.* Multiple orthoflaviviruses secrete sfRNA in mosquito saliva to promote transmission by inhibiting MDA5-mediated early interferon response. Preprint at https://doi.org/10.1101/2025.01.21.634113 (2025).

23. Slonchak, A. & Khromykh, A. A. Subgenomic flaviviral RNAs: What do we know after the first decade of research. *Antiviral Research* **159**, 13–25 (2018).

24. Rey-Cadilhac, F. *et al.* Characterization of size distribution and markers for mosquito extracellular vesicles. *Front. Cell Dev. Biol.* **13**, 1497795 (2025).

25. MacFadden, A. *et al.* Mechanism and structural diversity of exoribonuclease-resistant RNA structures in flaviviral RNAs. *Nat Commun* **9**, 119 (2018).

26. Chapman, E. G. *et al.* The Structural Basis of Pathogenic Subgenomic Flavivirus RNA (sfRNA) Production. *Science* **344**, 307–310 (2014).

27. Ward, A. M. *et al.* Quantitative mass spectrometry of DENV-2 RNA-interacting proteins reveals that the DEAD-box RNA helicase DDX6 binds the DB1 and DB2 3’ UTR structures. *RNA Biology* **8**, 14.

28. Baek, M. *et al.* Accurate prediction of protein–nucleic acid complexes using RoseTTAFoldNA. *Nat Methods* **21**, 117–121 (2024).

29. Jumper, J. *et al.* Highly accurate protein structure prediction with AlphaFold. *Nature* **596**, 583–589 (2021).

30. De Castro, E. *et al.* ScanProsite: detection of PROSITE signature matches and ProRule-associated functional and structural residues in proteins. *Nucleic Acids Research* **34**, W362–W365 (2006).

31. Mathur, G. *et al.* Transgene-mediated suppression of dengue viruses in the salivary glands of the yellow fever mosquito, *Aedes aegypti*. *Insect Molecular Biology* **19**, 753–763 (2010).

32. Martin, C., Ligat, G. & Malnou, C. E. The Yin and the Yang of extracellular vesicles during viral infections. *Biomedical Journal* **47**, 100659 (2024).

33. Dellar, E. R., Hill, C., Melling, G. E., Carter, D. R. F. & Baena-Lopez, L. A. Unpacking extracellular vesicles: RNA cargo loading and function. *J of Extracellular Bio* **1**, e40 (2022).

34. Corrado, C., Barreca, M. M., Zichittella, C., Alessandro, R. & Conigliaro, A. Molecular Mediators of RNA Loading into Extracellular Vesicles. *Cells* **10**, 3355 (2021).

35. Fabbiano, F. *et al.* RNA packaging into extracellular vesicles: An orchestra of RNA-binding proteins? *J of Extracellular Vesicle* **10**, e12043 (2020).

36. Villarroya-Beltri, C. *et al.* Sumoylated hnRNPA2B1 controls the sorting of miRNAs into exosomes through binding to specific motifs. *Nat Commun* **4**, 2980 (2013).

37. Temoche-Diaz, M. M. *et al*. Distinct mechanisms of microRNA sorting into cancer cell-derived extracellular vesicle subtypes. *eLife* **8**, e47544 (2019).

38. Iavello, A. *et al*. Role of Alix in miRNA packaging during extracellular vesicle biogenesis. *International Journal of Molecular Medicine* **37**, 958–966 (2016).

39. Janas, T., Janas, P., Sapoń, K. & Janas, T. Binding of RNA Aptamers to Membrane Lipid Rafts: Implications for Exosomal miRNAs Transfer from Cancer to Immune Cells. *IJMS* **21**, 8503 (2020).

40. Hagiwara, K., Katsuda, T., Gailhouste, L., Kosaka, N. & Ochiya, T. Commitment of Annexin A2 in recruitment of microRNAs into extracellular vesicles. *FEBS Letters* **589**, 4071–4078 (2015).

41. Nkosi, D. *et al.* Epstein-Barr Virus LMP1 Promotes Syntenin-1- and Hrs-Induced Extracellular Vesicle Formation for Its Own Secretion To Increase Cell Proliferation and Migration. *mBio* **11**, e00589-20 (2020).

42. Cone, A. S. *et al.* Alix and Syntenin-1 direct amyloid precursor protein trafficking into extracellular vesicles. *BMC Mol and Cell Biol* **21**, 58 (2020).

43. Li, L.-H. *et al.* A dengue type 2 reporter virus assay amenable to high-throughput screening. *Antiviral Research* **183**, 104929 (2020).

44. Li, L.-H. *et al.* Multiplexed multicolor antiviral assay amenable for high-throughput research. *Nat Commun* **15**, 42 (2024).

45. Kuno, G. Early History of Laboratory Breeding of *Aedes aegypti* (Diptera: Culicidae) Focusing on the Origins and Use of Selected Strains. *jnl. med. entom.* **47**, 957–971 (2010).

46. Rey-Cadilhac, F. *et al.* Characterization of size distribution and markers for mosquito extracellular vesicles. *Front. Cell Dev. Biol.* **13**, 1497795 (2025).

47. Liao, K.-C. *et al.* Identification and characterization of host proteins bound to dengue virus 3′ UTR reveal an antiviral role for quaking proteins. *RNA* **24**, 803–814 (2018).

48. Perez-Riverol, Y. *et al.* The PRIDE database at 20 years: 2025 update. *Nucleic Acids Research* **53**, D543–D553 (2025).

49. Baek, M. *et al.* Accurate prediction of protein–nucleic acid complexes using RoseTTAFoldNA. *Nat Methods* **21**, 117–121 (2024).

50. Sehnal, D. *et al.* Mol* Viewer: modern web app for 3D visualization and analysis of large biomolecular structures. *Nucleic Acids Research* **49**, W431–W437 (2021).

51. Horn, T. & Boutros, M. E-RNAi: a web application for the multi-species design of RNAi reagents—2010 update. *Nucleic Acids Research* **38**, W332–W339 (2010).

52. Blandin, S. A., Marois, E. & Levashina, E. A. Antimalarial Responses in Anopheles gambiae: From a Complement-like Protein to a Complement-like Pathway. *Cell Host & Microbe* **3**, 364–374 (2008).

53. Olmo, R. P. *et al.* Control of dengue virus in the midgut of *Aedes aegypti* by ectopic expression of the dsRNA-binding protein Loqs2. *Nat Microbiol* **3**, 1385–1393 (2018).

54. Marois, E. Techniques for Identifying and Sorting Transgenic Mosquito Larvae. *Cold Spring Harb Protoc* **2024**, pdb.top107694 (2024).

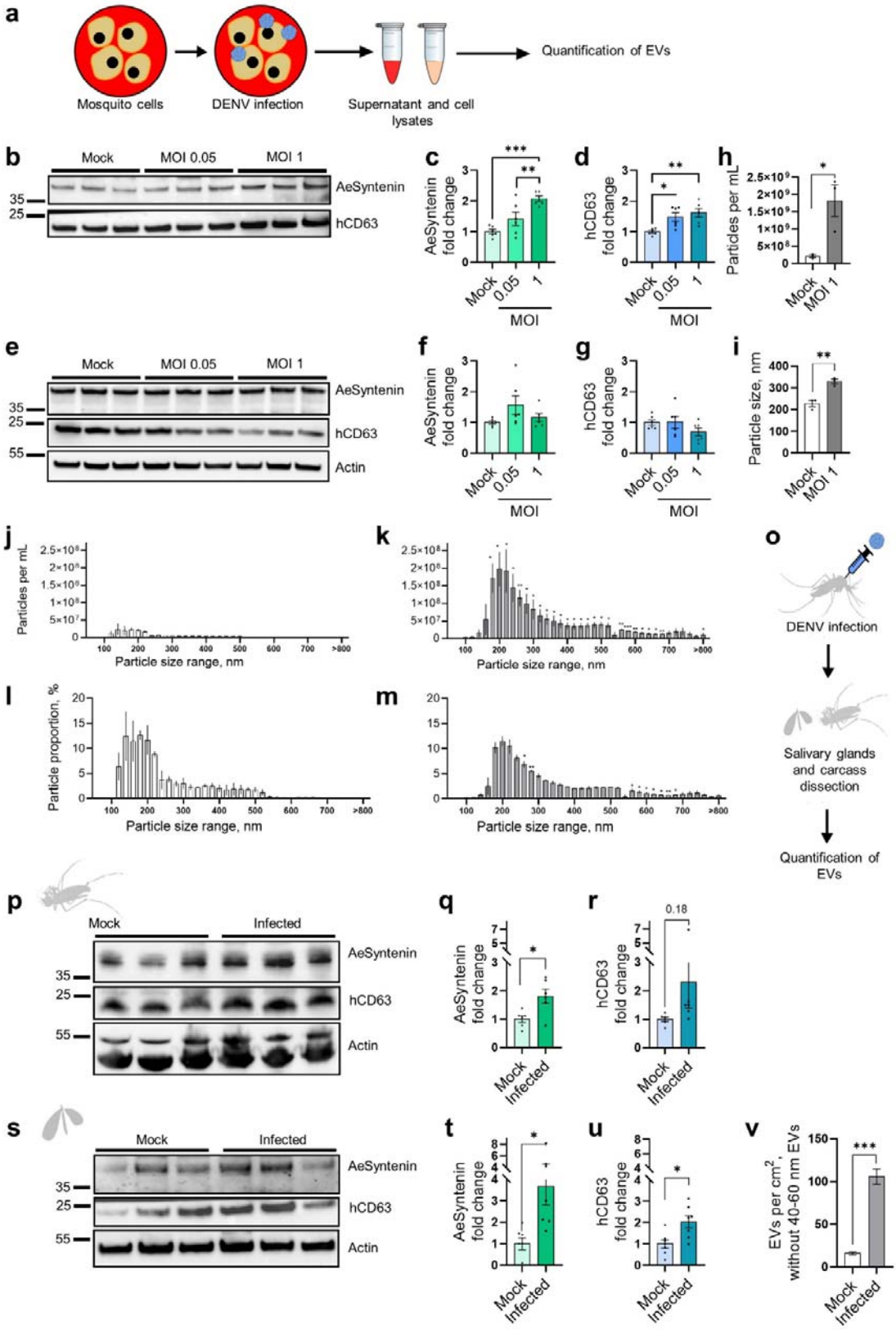
a
Mosquito cells
DENV infection
Supernatant and cell lysates
Quantification of EVs
b
Mock
MOI 0.05
MOI 1
AeSyntenin
hCD63
35
25
c
AeSyntenin fold change
Mock
0.05
1
MOI
d
hCD63 fold change
h
Particles per mL
Mock
MOI 1
e
Actin
55
f
g
i
Particle size, nm
j
Particles per mL
Particle size range, nm
k
o
DENV infection
Salivary glands and carcass dissection
Quantification of EVs
l
Particle proportion, %
m
p
Infected
q
r
0.18
s
t
u
v
EVs per cm², without 40-60 nm EVs

770

Fig. 1 | DENV infection stimulates secretion of EVs in cells and mosquitoes. a Assessing the effect of DENV infection on EV secretion in mosquito cells. **b-d** Representative WB (b) and quantification of AeSyntenin (c) and hCD63 (d) in media from cells infected with MOI 0.05 or 1. **e-g** Representative WB (e) and quantification of AeSyntenin (f) and hCD63 (g) in cells infected with MOI 0.05 or 1. Actin was used a loading control. **h,i** Particle concentration (h) and size (i) in media from cells infected with MOI 1 by NTA. **j-m** Size-range (20 nm width) particle concentration in media from cells mock-infected (j) and infected with MOI 1 (k), and size-range proportion in media from cells mock-infected (l) and infected with MOI 1 (m) by NTA. **o** Assessing the effect of DENV infection on EV secretion in mosquitoes. **p-r** Representative WB (p) and quantification of AeSyntenin (q) and hCD63 (r) in mock and infected carcasses. Actin was used as a loading control. **s-u** Representative WB (s) and quantification of AeSyntenin (t) and hCD63 (u) in mock and infected salivary glands. Five pairs of salivary glands were combined in each sample. Actin was used as a loading control. **v** EVs per cm^2 of pictures. n pictures, 40 and 35 for mock and infected saliva, respectively. Particles from 40-60 nm were not counted. c,d,f-m,q,r,t,u,v Bars represent mean ± s.e.m. and dots indicate repeats. j-m N, 3. c,d,f,g,h,i,q,r,t,u,v *, $p < 0.05$; **, $p < 0.01$; ***, $p < 0.001$, as determined by Fisher's LSD test or T-test. j-m *, $p < 0.05$ as determined by T-test in comparison with same size range in the corresponding mock condition.

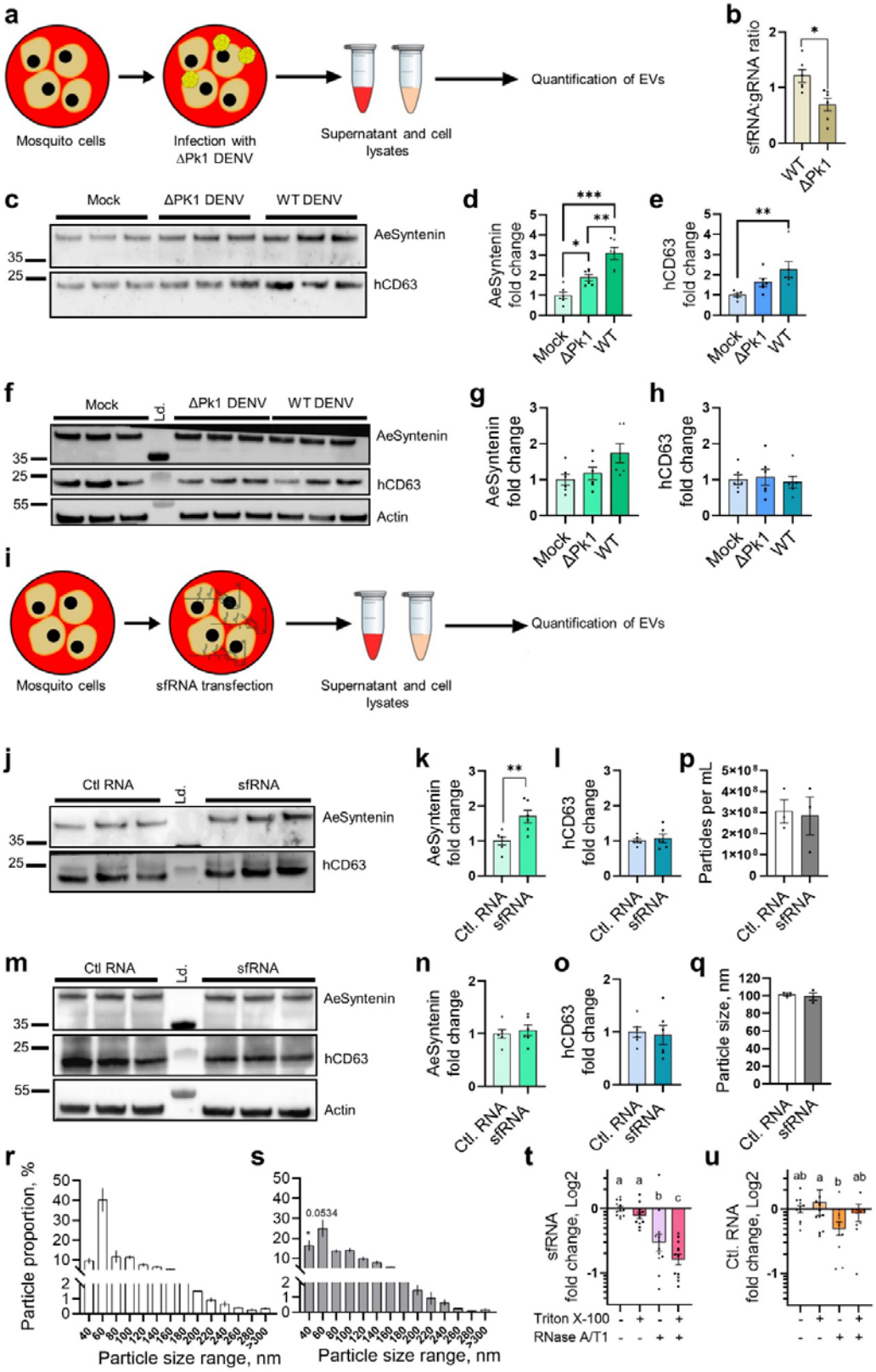
a
Mosquito cells
Infection with ΔPk1 DENV
Supernatant and cell lysates
Quantification of EVs
b
sfRNA:gRNA ratio
WT
ΔPk1
c
Mock
ΔPK1 DENV
WT DENV
AeSyntenin
hCD63
35
25
d
AeSyntenin fold change
Mock
ΔPk1
WT
e
hCD63 fold change
f
Mock
Ld.
ΔPk1 DENV
WT DENV
AeSyntenin
hCD63
Actin
55
g
h
i
Mosquito cells
sfRNA transfection
Supernatant and cell lysates
Quantification of EVs
j
Ctl RNA
sfRNA
k
l
p
Particles per mL
Ctl. RNA
m
n
o
q
Particle size, nm
r
Particle proportion, %
Particle size range, nm
s
0.0534
t
sfRNA fold change, Log2
Triton X-100
RNase A/T1
u
Ctl. RNA fold change, Log2

789

Fig. 2 | sfRNA stimulates secretion of EVs. a Assessing the effect of sfRNA-deficient DENV (ΔPk1 DENV) infection on EV secretion in mosquito cells. Control cells were infected with a wild-type infectious clone. **b** Levels of intracellular sfRNA:gRNA ratio. **c-e** Representative WB (c) and quantification of AeSyntenin (d) and hCD63 (e) in media from cells infected with mock, ΔPk1 and WT DENV. **f-h** Representative WB (f) and quantification of AeSyntenin (g) and hCD63 (h) in cells infected with mock, ΔPk1 and WT DENV. Actin was used as a loading control.. **i** Assessing the effect of sfRNA transfection on EV secretion in mosquito cells. A same-size viral RNA fragment was transfected as control (Ctl. RNA). **j-l** Representative WB (j) and quantification of AeSyntenin (k) and hCD63 (l) in media from cells transfected with sfRNA or Ctl. **m-o** Representative WB (m) and quantification of AeSyntenin (n) and hCD63 (o) in cells transfected with sfRNA or Ctl. RNA. Actin was used as a loading control. **p-q** Particle concentration (p) and size (q) in EVs isolated from cell media after transfection with sfRNA and Ctl. RNA. N, 3. **r,s** Size-range (20 nm width) particle proportion in media from cells transfected with Ctl. RNA (r) or sfRNA (s) by NTA. N, 3. **t,u** Levels of secreted RNase-resistant sfRNA (t) and Ctl. RNA (u) with or without Triton X-100 pre-treatment. b,d,e,g,h,k,l,n-u Bars show mean ± s.e.m. and dots indicate repeats. Ld., protein size ladder. g,h *, $p < 0.05$; **, $p < 0.01$; ***, $p < 0.001$, as determined by Fisher's LSD Test. N **, $p < 0.01$ as determined by T test. t,u Different letters indicate significant differences as determined by Fisher's LSD test.

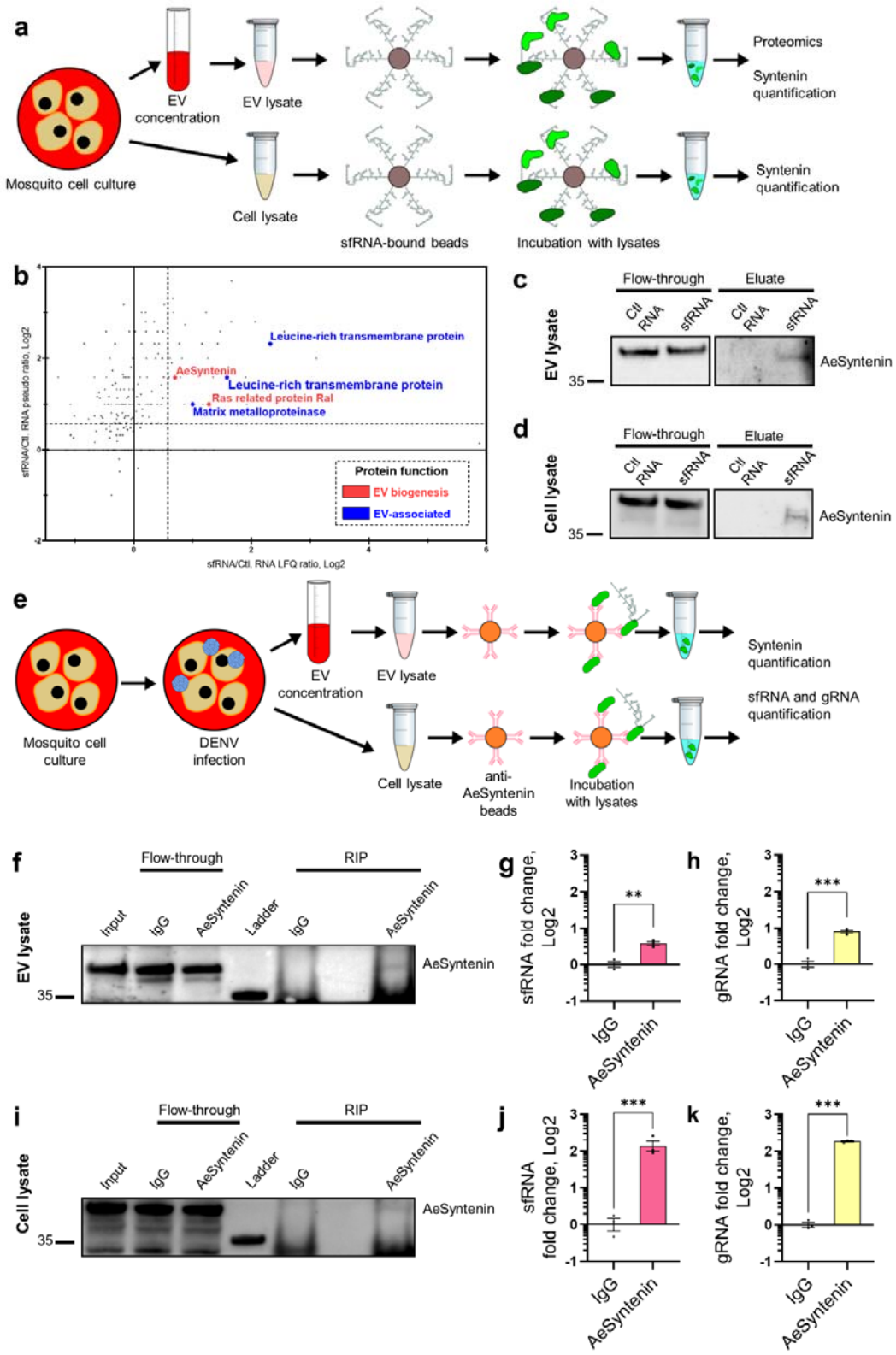
a
Mosquito cell culture
EV concentration
EV lysate
Cell lysate
sfRNA-bound beads
Incubation with lysates
Proteomics
Syntenin quantification
Syntenin quantification
b
Leucine-rich transmembrane protein
AeSyntenin
Leucine-rich transmembrane protein
Ras related protein Ral
Matrix metalloproteinase
Protein function
EV biogenesis
EV-associated
sfRNA/Ctl. RNA LFQ ratio, Log2
c
Flow-through
Eluate
Ctl RNA
sfRNA
EV lysate
AeSyntenin
35
d
Cell lysate
AeSyntenin
e
Mosquito cell culture
DENV infection
EV concentration
EV lysate
Cell lysate
anti-AeSyntenin beads
Incubation with lysates
Syntenin quantification
sfRNA and gRNA quantification
f
RIP
Input
IgG
AeSyntenin
Ladder
g
sfRNA fold change, Log2
h
gRNA fold change, Log2
i
Cell lysate
j
sfRNA fold change, Log2
k
gRNA fold change, Log2

809

810

Fig. 3 | sfRNA interacts with AeSyntenin.

a Identification of sfRNA-interacting proteins by RNA-affinity chromatography. A same-sized viral control RNA (Ctl RNA) fragment was used as control. **b** Label free quantification (LFQ) and pseudo ratio for sfRNA-interacting proteins as determined by MS analysis. Proteins with putative functions associated with EVs, EV biogenesis, RNA binding or Golgi trafficking are identified with different colors. **c, d** AeSyntenin detection in flow-through and eluate from RNA-affinity chromatography conducted with EV (c) and cell (d) lysates. **e** Identification of AeSyntenin-interacting viral RNAs in EVs and cells infected with DENV by RNA immunoprecipitation. **f-h** Syntenin detection (f) in flow-through and RNA immunoprecipitates (RIP), sfRNA (g) and gRNA (h) levels precipitated with anti-AeSyntenin and IgG control in EV lysates. **i-k** AeSyntenin detection (i) in flow-through and RNA immunoprecipitates (RIP), sfRNA (j) and gRNA (k) levels precipitated with anti-AeSyntenin and IgG control in cell lysates. g,h,j,k Bars represent mean ± s.e.m. Dots indicate repeats. **, $p < 0.01$; ***, $p < 0.001$, as determined by T test.

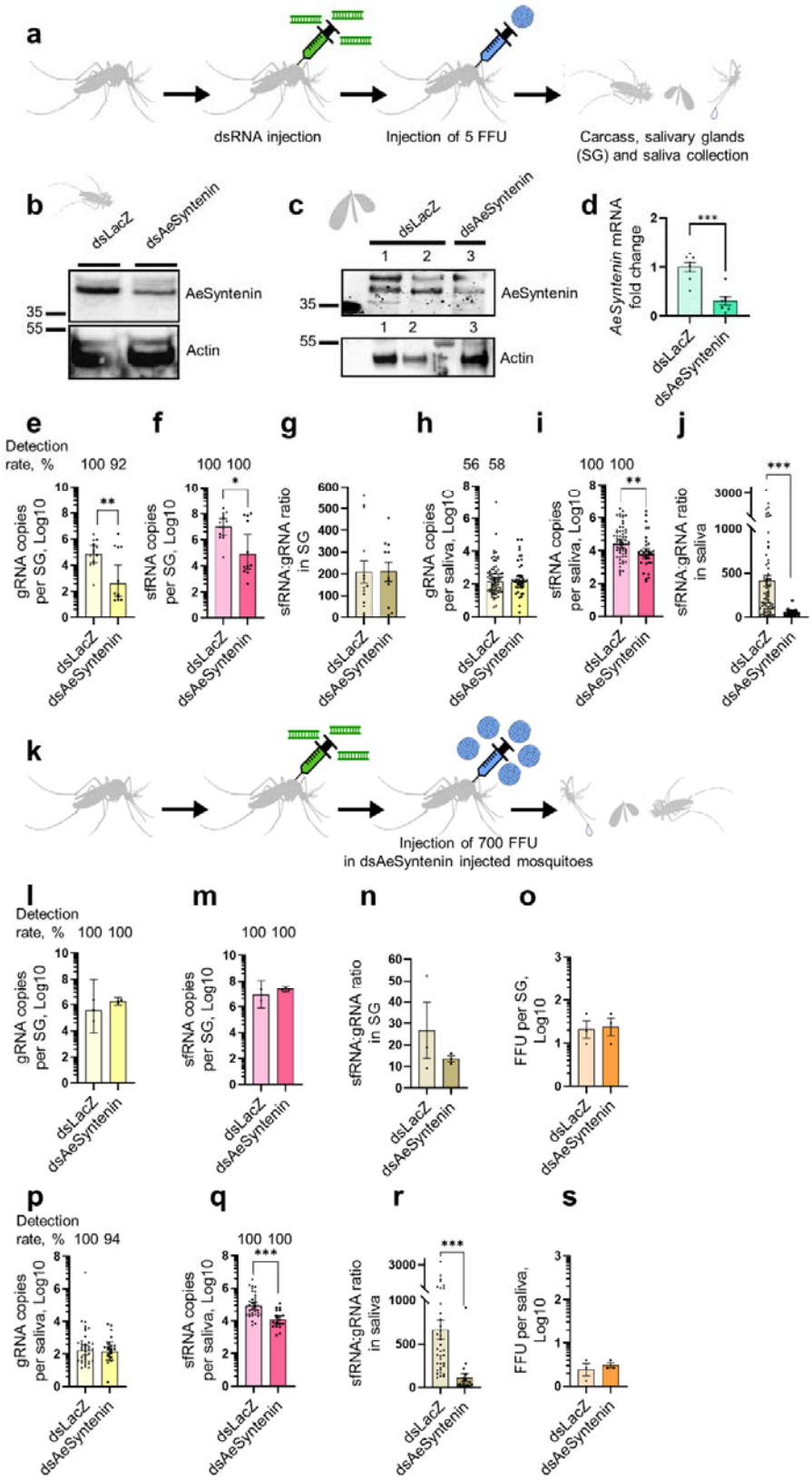
a
dsRNA injection
Injection of 5 FFU
Carcass, salivary glands (SG) and saliva collection
b
dsLacZ
dsAeSyntenin
AeSyntenin
Actin
35
55
c
dsLacZ
dsAeSyntenin
1 2 3
AeSyntenin
Actin
35
55
d
AeSyntenin mRNA fold change
***
dsLacZ
dsAeSyntenin
e
Detection rate, %
100 92
gRNA copies per SG, Log10
**
f
100 100
sfRNA copies per SG, Log10
*
g
sfRNA:gRNA ratio in SG
h
56 58
gRNA copies per saliva, Log10
i
100 100
sfRNA copies per saliva, Log10
**
j
sfRNA:gRNA ratio in saliva
***
k
Injection of 700 FFU in dsAeSyntenin injected mosquitoes
l
Detection rate, %
100 100
gRNA copies per SG, Log10
m
100 100
sfRNA copies per SG, Log10
n
sfRNA:gRNA ratio in SG
o
FFU per SG, Log10
p
Detection rate, %
100 94
gRNA copies per saliva, Log10
q
100 100
sfRNA copies per saliva, Log10
***
r
sfRNA:gRNA ratio in saliva
***
s
FFU per saliva, Log10

826

Fig. 4 | AeSyntenin depletion in mosquitoes reduces sfRNA secretion in saliva. a Assessing the effect of AeSyntenin depletion on gRNA and sfRNA levels in carcasses, salivary glands (SG) and saliva. Mosquitoes were injected with dsRNA against AeSyntenin or LacZ as control before inoculation with 5 FFU of DENV. **b,c** AeSyntenin levels in carcass (b) and in SG (c). Actin was used as a loading control. **d** *AeSyntenin* mRNA levels in SG. **e-g** Levels of gRNA (e), sfRNA (f) and sfRNA:gRNA ratio (g) in SG. **h-j** Levels of gRNA (h), sfRNA (i) and sfRNA:gRNA ratio (j) in saliva. **k** Assessing the effect of AeSyntenin depletion on gRNA and sfRNA levels in carcasses, salivary glands (SG) and saliva after compensating for AeSyntenin effect on SG infection levels. Mosquitoes injected with dsAeSyntenin were inoculated with 700 FFU of DENV, whereas mosquitoes injected with dsLacZ were injected with 5 FFU. **k-o** Levels of gRNA (k), sfRNA (m), sfRNA:gRNA ratio (n) and infectious particles (o) in SG. **p-s** Levels of gRNA (p), sfRNA (q), sfRNA:gRNA ratio (r) and infectious particles (s) in saliva. d,g,j,n,o,r,s Bars represent mean ± s.e.m. and dots indicate repeats. e,f,h,u,l,m,p,q Bars represent geometric mean ± 95% C.I. and dots indicate repeats. FFU, focus forming unit. *, $p < 0.05$; **, $p < 0.01$; ***, $p < 0.001$, as determined by T-test.

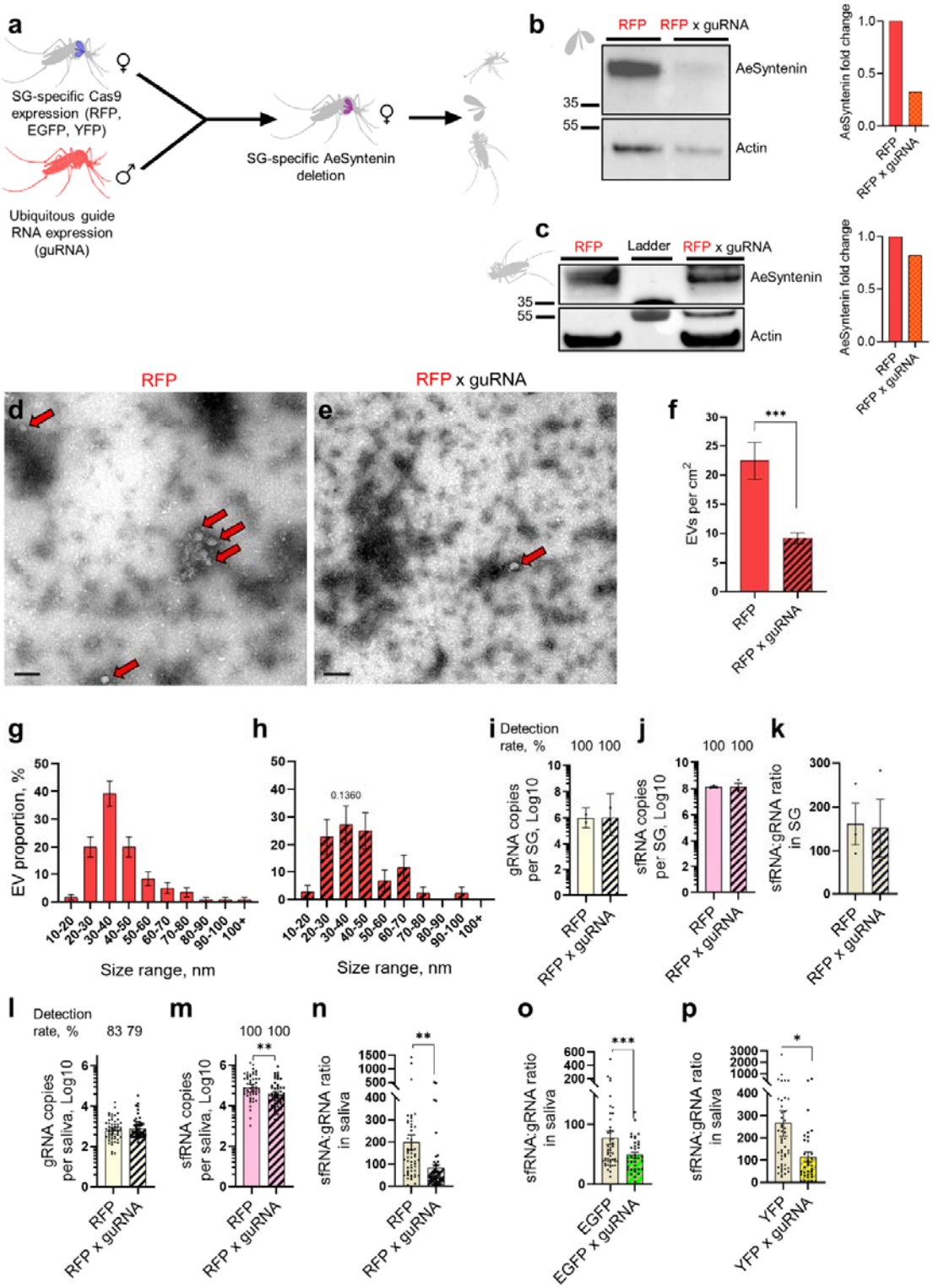

Fig. 5 | AeSyntenin genetic deletion in salivary glands reduces EVs and sfRNA in saliva.

a Production of SG-specific AeSyntenin deletion mosquitoes. **b,c** AeSyntenin detection in SG

(b) and carcass (c) from control RFP and RFP x guide RNA (guRNA) progeny. Bar graphs show AeSyntenin fold change normalized to Actin. **d-f** Representative TEM pictures of saliva from RFP (d) and RFP x guRNA progeny (e), and EVs per cm^2 of pictures (f). Scale bar, 100 nm. Red arrows indicate EVs. EV concentration was calculated from 34 and 35 pictures for RFP and RFP x guRNA, respectively. **g,h** Distribution of EVs per size range in RFP (g) and RFP x guRNA progeny (h). N EVs for g, 120; and for h, 44. **i-k** Levels of gRNA (i), sfRNA (j) and sfRNA:gRNA ratio (k) in SG from infected RFP and RFP x guRNA progeny. **l-n** Levels of gRNA (l), sfRNA (m) and sfRNA:gRNA ratio (n) in saliva from infected RFP and RFP x guRNA progeny. **o,p** Levels of sfRNA:gRNA ratio in saliva from infected EGFP and EGFP x guRNA progeny (o) and YFP and YFP x guRNA progeny (p). f,k,n,o,p Bars represent mean ± s.e.m. and dots indicate repeats. g,h Bars show proportion ± SD. i,j,l,m Bars represent geometric mean ± 95% C.I. and dots indicate repeats. f,m-p *, $p < 0.05$; *, $p < 0.01$; ***, $p < 0.001$ as determined by T test. h *, $p < 0.05$ as determined by Z test with same size range in RFP.